# Patterns for gridshells with negligible geometrical torsion at nodes

Xavier Tellier, Romane Boutillier, Cyril Douthe, Olivier Baverel

# Patterns for gridshells with negligible geometrical torsion at nodes

Xavier TELLIER[a], Romane BOUTILLIER[a], Cyril DOUTHE[a], Olivier BAVEREL[a]

[a] *Laboratoire Navier – UMR8205, Ecole des Ponts ParisTech, Univ Gustave Eiffel, CNRS, France (xavier.tellier@enpc.fr)*

## Abstract

Curved envelope structural building envelopes have been quite popular in architecture in the past decades, and pose many challenges in their design, manufacturing and planning. In gridshells, a popular structural morphology for curved structure, designers will often strive to orient beams such that their top face is parallel to the envelope surface. However, this tends to induce geometrical torsion along the beam centerline, which complexifies significantly the manufacturing of the connection nodes or of the beams themselves. It is well known that such issue can be avoided by aligning beams with principal curvature directions of the envelope surface, thus yielding a quadrangular paneling. In this article, we study how other types of patterns (non-quadrangular) can be used to design torsion-free gridshells. Based on asymptotic considerations, we derive a set of geometrical rules which, if fulfilled by a pattern, insure that a surface can be covered by this pattern with negligible torsion and limited deviation of beams from surface normals.

We show that a wide variety of patterns fulfill these rules, offering interesting possibilities for the design of curved architectural envelopes (Figure 1). As these rules are based on first order asymptotic analysis, we perform global validation on case studies. One main application is for structures in which face planarity is not necessary, for example ones cladded with ETFE cushions.

**Keywords**: Architectural geometry, gridshells, patterns

*Paper included in the Special Issue entitled: Shell and Spatial Structures: Between New Developments and Historical Aspects*

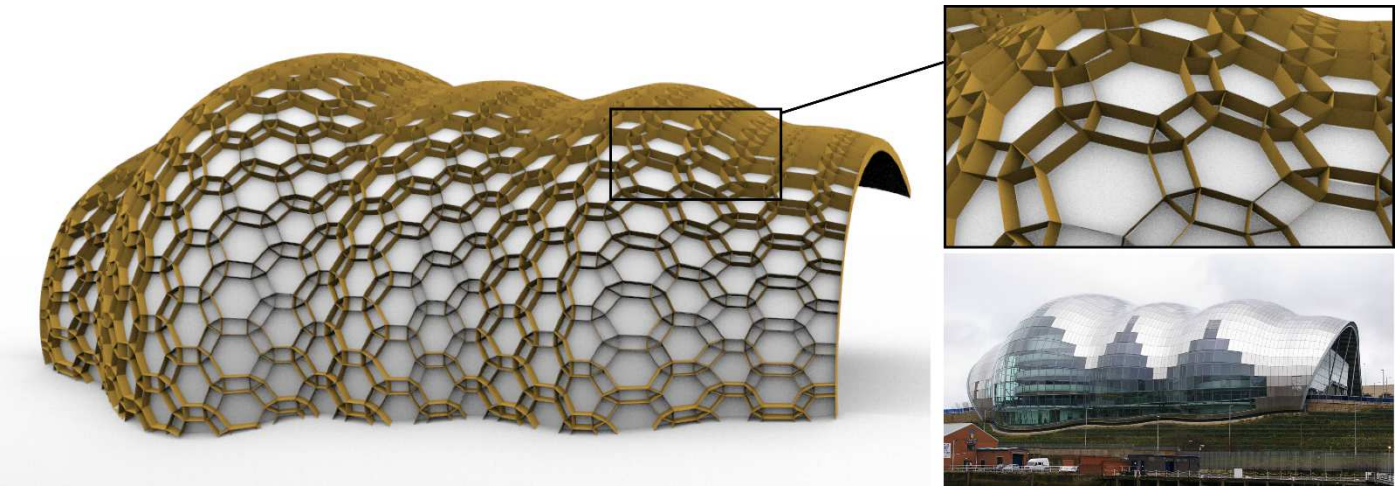

Figure 1. An alternative panelization of the SAGE music center with an Archimedean hex-quad-tri tiling. Compared to the original design by F+P, faces are no longer planar, but nodes are still free of geometrical torsion (with 0.5° tolerance), while node axes remain on average within 2° of surface normal (bottom right picture © W. Nicholson).

# 1. Introduction

## 1.1. Incentive of the research

Double curvature can make a structural envelope expressive architecturally and, at the same time, highly efficient mechanically, thus reducing the amount of material and the environmental footprint of the building. One main limitation of the use of curved envelopes is the fabrication complexity they involve, which tends to increase drastically their cost. For a gridshell (a grid acting mechanically as a shell), the most challenging manufacturing task is the connections, between beams and between panels and beams.

Beam-panel connections can be significantly simplified if the beams top surface is parallel to the tangent plane of the envelope surface – otherwise, a high kink angle appears between panels and beams, a problem discussed in [1]. This property also improves the mechanical efficiency of the beams against the wind load and improves light transmission.

However, aligning the beam top face with the surface often results in geometrical torsion, as the normal vector along a curve on a surface undergoes twisting. Such a torsion can significantly complicate the connection between beams (note: in this article, by *torsion*, we will always refer to this type of torsion, and not to torsion as a beam stress).

There are three strategies that deal with these two considerations:

**Strategy #1** consists of orienting beam sections with surface normals, and accommodating torsion in beams (by twisting them, or using circular pipe profiles) or at nodes between beams. Examples are shown in the top row of Figure 2.

**Strategy #2** sets all beams in a vertical plane, so that beams can be connected without torsion. However, this results in high kinks between the envelope surface and beams when the slope is elevated (Figure 2, bottom left).

**Strategy #3** consists of searching for the beam orientations that fulfill at best the two above properties by optimization of the section orientation. This approach is particularly suited for gridshells with straight bars. It is known to work well for quadrangular meshes aligned with principal curvature directions.

This article proposes to enrich strategy #3 by studying other periodic patterns.

Generally, torsion is considered along with face planarity. Face planarity is a strong constraint, which in particular causes faces to be non-convex in saddled-shaped meshes with 3-valent nodes. Here, we consider torsion alone, without consideration of face planarity. This work is hence well suited for cladding techniques that do not require face planarity, such as ETFE (éthylène tétrafluoroéthylène) cushions or folded panels. More precisely, we propose a set of geometrical rules to select and orient patterns so that strategy #3 is highly likely to succeed. This set of rules is presented in section 2, along with its theoretical basis, and is validated numerically with case studies in section 3.

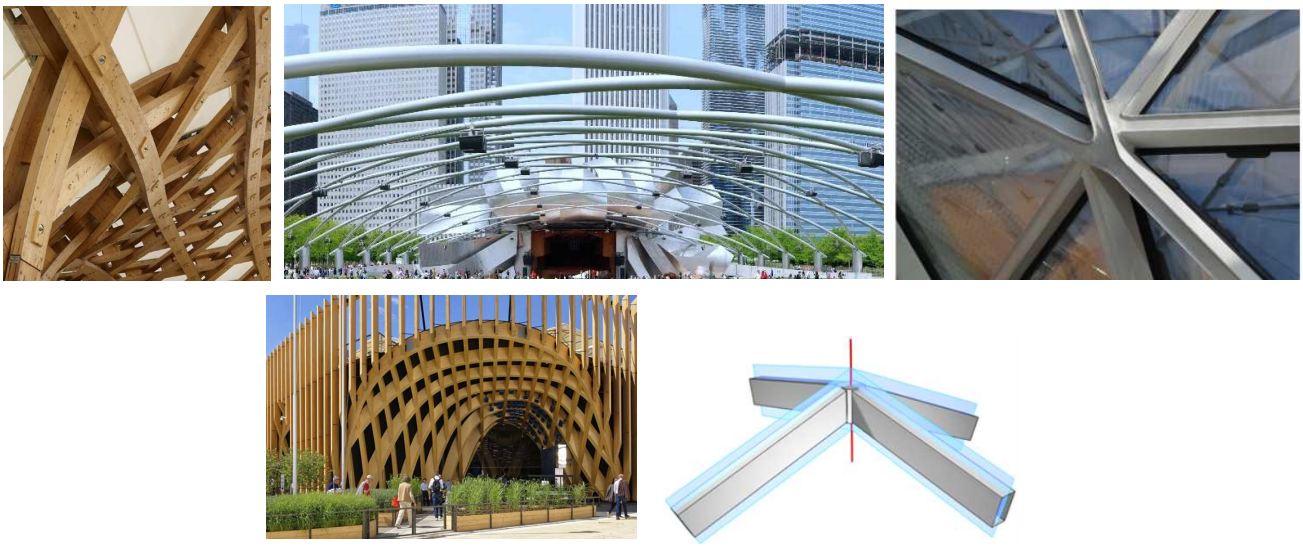

Figure 2. Common strategies to deal with geometrical torsion

Top row: strategy #1. Left: Centre Pompidou Metz (©D. Boy de la Tour) ; Middle: Jay Pritzker Pavilion ; Right : MyZeil shopping mall (©R. Mesnil).

Bottom left: strategy #2, France Pavilion at Milan World Expo (©Simonin). Bottom right: strategy #3

### 1.2. Context and brief literature review

#### Torsion-free gridshells

The consequences of geometrical torsion on detailing of gridshell nodes are presented in [2]. Geometries with torsion-free nodes have been addressed in the literature in the context of circular meshes [3], conical meshes [4], edge offset meshes, Caravel meshes [5] and honeycomb structures [6]. [7] proposes a generation method for 3-valent patterns based on Voronoi diagrams, and shows application to the realization of the mock-up of curved objects..

In this paper, we account for the fabrication tolerances for the beams sections to deviate from the surface normals. The use of fabrication tolerances to design near torsion-free gridshells was approached in [8].

#### Gridshell patterns

A study of the generation of various periodic patterns is made in [9] with the constraint of face planarity, and with a focus on having a fair mesh and symmetric nodes in [10]. Torsion-free structures with various repetitive patterns are constructed from circle-packings in [11]. Some popular patterns are compared in [12], [13] relatively to their structural resistance.

## 2. A simple rule for designing torsion-free patterns

In this section, we give a set of rules that guarantee that a pattern can be realized as a torsion-free gridshell with low deviation of beam sections from the envelope surface. These rules are based on an asymptotic case: we consider the situation in which a smooth surface is approximated by a mesh in which edge lengths are much smaller than the curvature radii of the surface. In that setting, the neighborhood of a point on the surface is planar at the first order and the variations of the normal vectors are also contained in a plane. We thus linearize the differential problem underlying geometrical fabrication constraints.

## 2.1. Visualizing strategies to deal with torsion using the Gauss map

### Linearized Gauss map

Let us start by recalling some concepts of surface geometry. Let us consider a point $P$ on a smooth surface, as shown in Figure 3. The unit normal at $P$, called the Gauss map of $P$, $\boldsymbol{n}(P)$, can be described by a point on the unit sphere. Considering a small displacement $\boldsymbol{u}$ on the surface, $P + \boldsymbol{u}$ is at the first order included in the tangent plane at $P$, $T_P$. The variation of the normal from $P$ to $P + \boldsymbol{u}$ is at the first order a vector of the tangent plane of the sphere at $\boldsymbol{n}(P)$. We identify this tangent plane $T_{NP}$ with $T_P$. The variation of the normal at $P$ is then given by the shape operator of the surface, which can be expressed as a linear map on $T_P$ [14]:

$$\boldsymbol{dn}(\boldsymbol{u}) = -\begin{bmatrix} k_1 & 0 \\ 0 & k_2 \end{bmatrix}\begin{pmatrix} u_1 \\ u_2 \end{pmatrix}$$

where $\boldsymbol{u} = u_1\boldsymbol{e_1} + u_2\boldsymbol{e_2}$ is the decomposition of $u$ in the basis of principal curvature directions $(\boldsymbol{e_1}, \boldsymbol{e_2})$ of $T_P$.

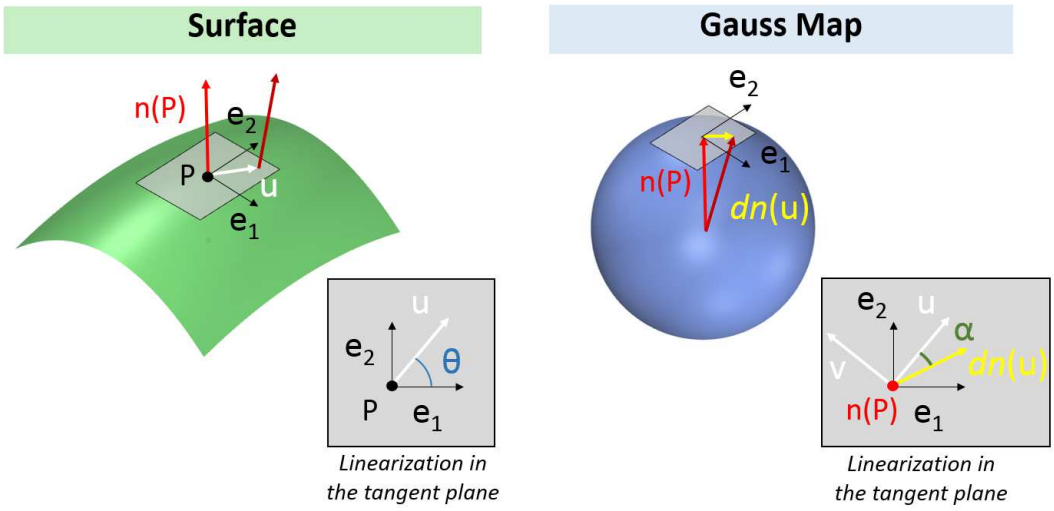


Figure 3. Gauss map of a smooth surface

The shape operator can be interpreted as a combination of two 1D-scalings of the tangent plane at $P$, respectively in the directions $\boldsymbol{e_1}$ and $\boldsymbol{e_2}$, with factors $-k_1$ and $-k_2$. As we will consider structures in which node axes do not coincide with the normal vectors of the envelope surface, we will use the upper case $\boldsymbol{N}$ to designate a node axis, and the lower case $\boldsymbol{n}$ to designate the surface normal, as illustrated in Figure 4.

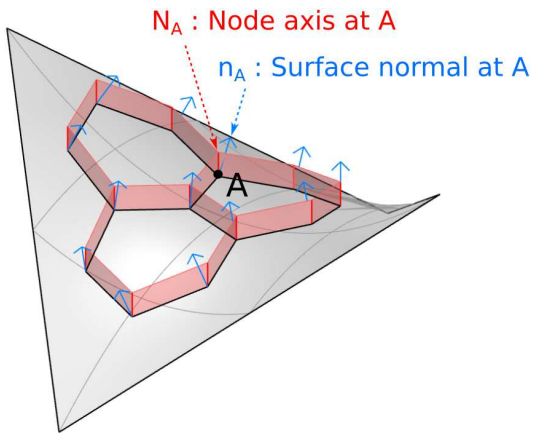


Figure 4. Node axis and surface normals

**Asymptotic pattern behavior**

In our asymptotic approach, we consider patterns with edges much shorter than curvature radii. We will assume that in the limit case, the pattern is locally planar and periodic on the surface. The Gauss image of the pattern is then also a planar periodic pattern. This is illustrated in Figure 5: a periodic pattern on the surface is shown in black (left), and its Gauss image is shown in blue (it is identical on the right three pictures). The orientation of the node axes of the structure (vectors $\boldsymbol{N}$) is also a periodic pattern in this asymptotic case. It can be represented by a pattern on the tangent plane to the unit sphere (red patterns of the right three pictures).

**Visualization of pattern torsion on the Gauss map**

The above linearized point of view can be used to describe the strategies to deal with node torsion mentioned in section 1 (Figure 5). Depending on the strategy, the differences between the red pattern (which represent node axes in the actual structure) and the blue one (which represents surface normals) can be used to visualize both the torsion at nodes and the deviation from surface normal, as will be detailed further in the text.

**Strategy #1** (Aligning node axes with surface normals) In this case, the node axis (in red) of any point (e.g. $\boldsymbol{C}$ ) coincides with the surface normal ($\boldsymbol{n(C) = N(C)}$). The torsion along a bar can be obtained from the angle between its center line and its Gauss map (angle $\boldsymbol{\alpha}$ on Figure 5). For this purpose, we introduce the vector $\boldsymbol{v}$ normal to both $\boldsymbol{u}$ and $\boldsymbol{n}$ (see Figure 3), such that $(\boldsymbol{u, v, n})$ is the Darboux frame defined by the motion of $\boldsymbol{P}$ on the surface. The geodesic torsion of the Darboux frame is [14]:

$$\boldsymbol{\tau = dn(u).v = \sin\alpha\ \|dn(u)\| = \sin\alpha\ \sqrt{k_1^2\cos^2\theta + k_2^2\sin^2\theta}}$$

Where $\boldsymbol{\theta = e_1 \angle u}$.

**Strategy #2** (Set all axes in a fixed direction) In that case, for any point on the surface, the axis is at the same point on the Gauss map. There is hence a dissociation of the surface normals $\boldsymbol{n}$ from the node axes $\boldsymbol{N}$ (Figure 4). The angle between the two at a given point $\boldsymbol{C}$ is the geodesic distance on the sphere between $\boldsymbol{n(C)}$ and $\boldsymbol{N(C)}$. This angle gives the deviation of the beam top face compared to the surface.

**Strategy #3** (Optimize torsion-free axes to fit normals) Figure 5 (right) shows how node axes can be chosen in a torsion free configuration (e.g. the absence of torsion from A to B is guaranteed by the fact that $\boldsymbol{\overrightarrow{AB} || \overrightarrow{N(A)N(B)}}$, such that the node axes are much closer to the surface normals compared to strategy 2 (the distance $\boldsymbol{n(C)}$ to $\boldsymbol{N(C)}$ is much lower).

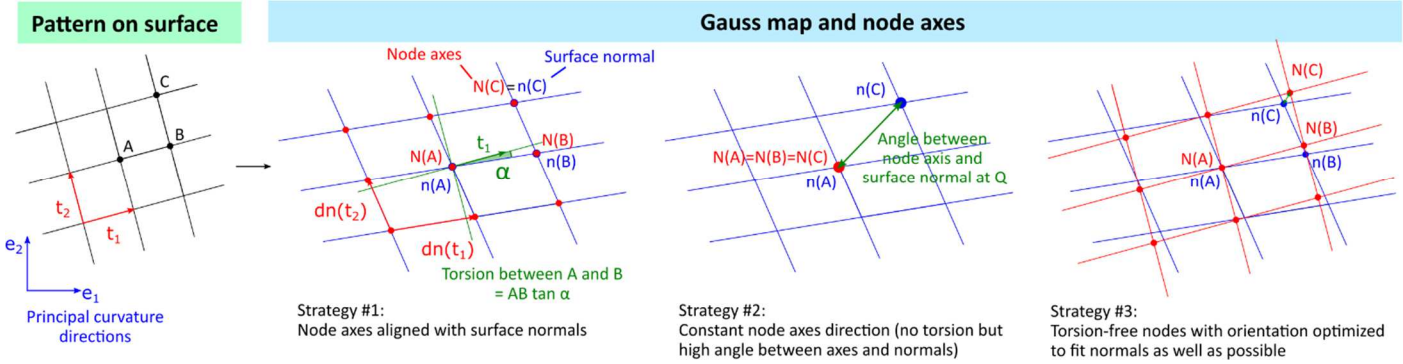


Figure 5. Visualization of the three strategies to deal with torsion on the linearized Gauss map

### 2.2. A sufficient rule for low torsion

Strategy 3 gives an interesting trade-off compared to strategies 1 and 2. However, the optimization might yield limited improvements, with axes that still deviate significantly from surface normals. This can be observed in **Figure 5** (right): as we move away from point A, the distance between $\boldsymbol{n}$ and $\boldsymbol{N}$ (i.e. the angle between axes and normal) keeps increasing, such that high kinks between panels and beams will be unavoidable far away from A. In the ordinary case, there is thus an accumulation of deviation between axes and surface normals.

The investigation of the origin of this accumulation has shown that it can be prevented at the first order if the pattern verifies certain rules. These rules build on the periodicity of the pattern (rule 1), the nature of the pattern and its local scalability so that its size can be adjusted with the curvature ratio (rule 2) and the alignment of the periodic pattern with principal curvature lines (rule 3). They can be formulated mathematically as follow :

**A sufficient set of rules to guarantee negligible torsion:**

1/ The pattern, when tiling the Euclidian plane, is periodic in two orthogonal directions. This means that there exists two orthogonal vectors $\boldsymbol{t_1}$ and $\boldsymbol{t_2}$ such that the pattern is invariant by a translation by either of these two vectors.

2/ There exists a parallel transformation[1] in the plane of the pattern that results in a tiling with periods $\boldsymbol{t_1}$ and $\lambda\boldsymbol{t_2}$, where $\lambda$ is an arbitrary number verifying $\lambda \neq 1$.

3/ At any point of the surface, periodicity directions $\boldsymbol{t_1}$ and $\boldsymbol{t_2}$ are aligned respectively with the principal curvature directions $\boldsymbol{e_1}$ and $\boldsymbol{e_2}$ of the surface.

The most simple torsion-free structure - quadrangles aligned with principal curvature directions – fulfills this set of rules. Supposing that curvature directions are horizontal and vertical, the octo-quad pattern of Figure 6 also fulfills them: the entire pattern can be obtained by copying and translating the square primitive cell in dashed red (rule 1/), and there exists a parallel transformation of the pattern inside the cell that results in a horizontal elongation of the cell boundary (rule 2/). The fact that the transformation is indeed parallel can be observed by following the colored lines (orange, blue, green and purple) during the transformation: its length changes, but not its orientation. Regarding rule 2/, we can observe on Figure 6 that finding one value of $\lambda$ implies that we can find any other values of $\lambda$, even though this might result in edges changing orientation (far right picture, colors).

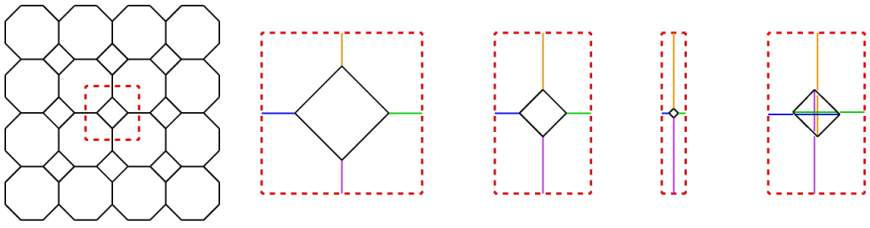

Figure 6. Supposing that curvature directions are horizontal and vertical, the Archimedian octo-quad tiling fulfills the rules.

Figure 7 proves on an example how, based on our hypothesis of asymptotic pattern behavior, the combination of the three rules allows the node axes to remain close to surface normals while still having no torsion:

[1] A parallel transformation conserves the orientation and connectivity of a pattern, but modifies edge lengths.

- The black pattern on the surface is deformed into the red one on the Gauss map by a parallel transformation. This guarantees the absence of node torsion.
- Thanks to rules 1/ to 3/, we found such a parallel transformation that yields node axes (red pattern) which have the same periodicity as the surface normals (blue pattern, with periodicity $\boldsymbol{dn(t_1)}$ *and* $\boldsymbol{dn(t_2)}$). We observe that node axes do deviate from the surface normals ($\boldsymbol{N}(A) \neq \boldsymbol{n}(A)$), but the deviation is identical for two adjacent cells. There is hence no accumulation of deviation from one cell to the other.

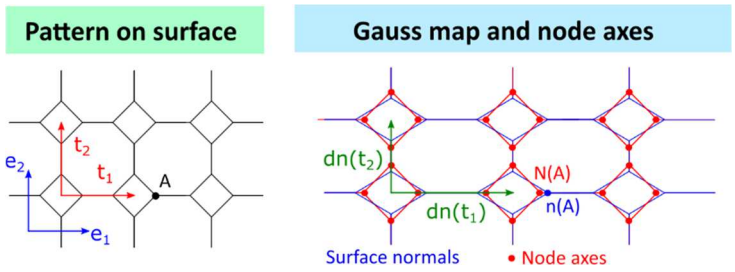


Figure 7. As this octo-quad pattern fullfills the rules, the angle between node axes and surface normals do not increase as we move away from A

**Examples**

All the patterns of Figure 8 Figure 8 verify the rules. Parallel deformation modes are shown below for each pattern. We can observe the great variety of patterns which fulfill them. Counter-examples are given in Figure 9. In pattern a., periodicity directions are not orthogonal. After a shear deformation (pattern b.), orthogonal periodicity directions can be found, but all the parallel transformations conserve the aspect ratio of the primitive cell because of the diagonal. The same thing is true for patterns c. and d.: a parallel transformation that modifies the aspect ratio of the primitive cell cannot be found, hence they do not fulfill the rules.

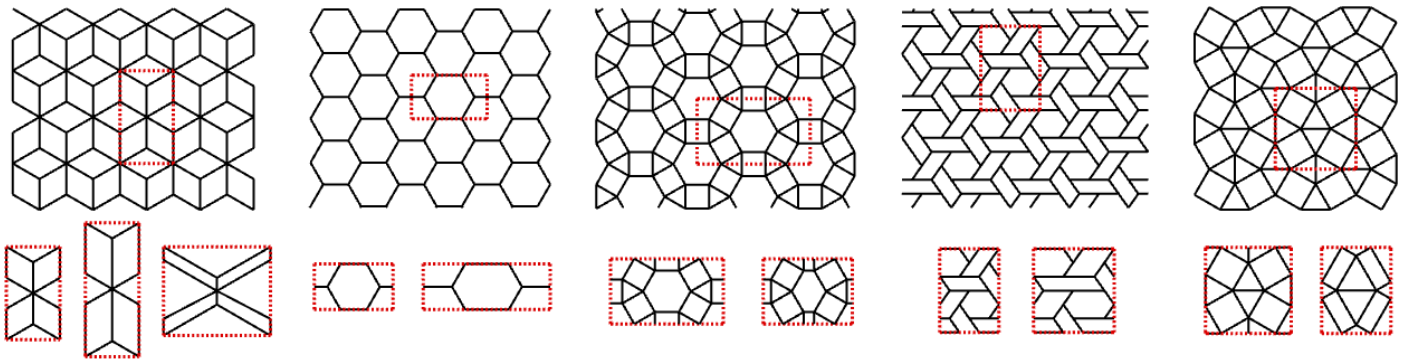

Figure 8. More patterns fulfilling the rules

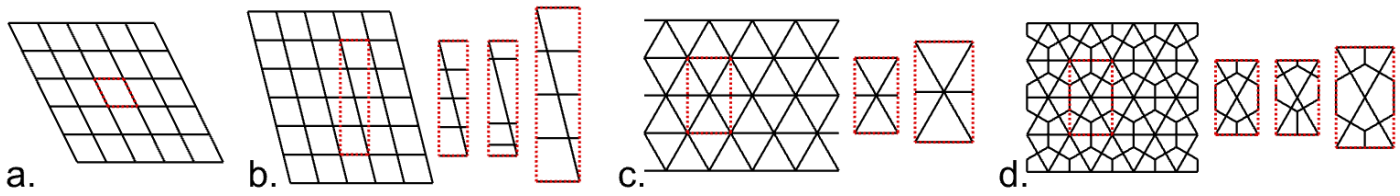


Figure 9. Counter-examples: these patterns do not fulfill the rules

**A not-necessary rule**

Planar hexagonal meshes not aligned with principal direction do not fulfill the rule: their primitive cell is not rectangular in the tangent plane. However, they can still be designed with low torsion and limited node axis deviation from surface

normals – the node axis being the intersection of the bisector planes of the faces adjacent to a node. Hence, this set of rules is sufficient, but not necessary.

## 3.Method validation

### 3.1. Methodology

As the proposed rule is based on local asymptotic analysis, this section studies its validity on a global scale. For this purpose, we perform case studies on meshes covering reference surfaces. We compare numerically three pairs of patterns with similar connectivity and edge lengths, one fulfilling the rules, the others not. We optimize the node axes orientation to obtain torsion-free gridshells and we then compare the deviation of the node axes with the surface normals.

### 3.2. Patterns

The three pairs of patterns used for the comparison are shown in Figure 10. The fulfillment of rules is investigated supposing that curvature directions are horizontal and vertical. In the first pair *(a,b)*, the two patterns have the same geometry, but are aligned differently on surfaces. Pattern *a* will be aligned with principal curvature directions, while pattern *b* will be at 45°. In the second pair *(c,d)*, the two patterns have the same average orientation with respect to principal curvature directions. They also have the same connectivity. However, pattern *d* is composed of collinear edges, such that it does not fulfill the rules, while pattern *c* has zigzags that make it fulfill the rules (the square primitive cell is highlighted in red). In the last pair *(e,f),* the two patterns have the same orientation and the same set of faces (two triangles for one hexagon). However, their connectivity is different, so that pattern *e* fulfills the rules, but not pattern *f* (which is known as a Kagome pattern).

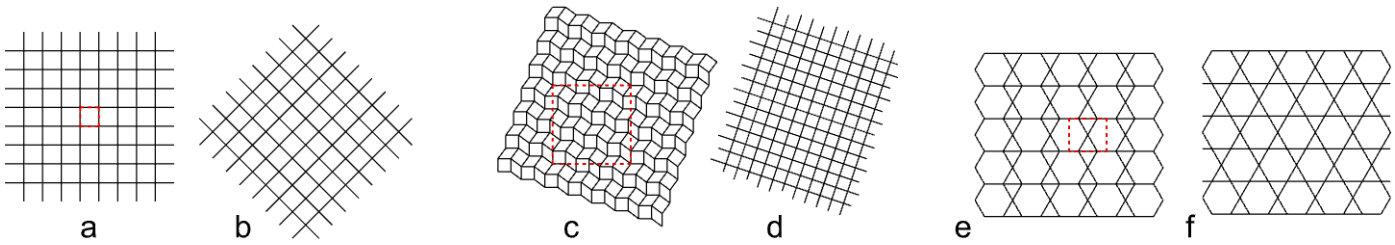


Figure 10. Patterns to be compared. Left: same pattern, aligned or not with principal curvature directions. Middle: Two patterns with same connectivity. One has kinks such that it fulfills the rules. Right: Two Archimedean patterns based on hexagons and triangles, only the left one fulfills the rules.

### 3.3. Reference surfaces

We use two reference surfaces to compare the patterns, visible on Figures 11 and 12. The first one is a Monge surface in which the two guide curves are Euler spirals. This insures a high dispersion of the principal curvatures on the surface. The second is a cylinder. It has a constant curvature and thus can result in a high accumulation of deviation between nodes axes and surface normals if a pattern does not fulfill the rules (cf discussion in section 2.2).

### 3.4. Generation method

We generate torsion-free meshes with the following steps:

1. Patterns are mapped to the reference surfaces following curvature lines without knowledge of the parallel transformation (the relative distance are kept elastic and part of the optimisation process).

2. Normals are initialized using the surface normals.
3. Orientation of normals is optimized using Kangaroo2 (that is based on the projection-based optimization algorithm presented in [15]) to minimize torsion. We stop the optimization when the maximum torsion has reached 0.5°. This convergence criterion comes from the fact that construction tolerances usually allow for some torsion so that nodes need not be exactly torsion-free. It can naturally be adapted depending on the admissible tolerances (see section 4.2).

Note that, in this optimisation process, the positions of the nodes on the surface and the node orientations are both variable. However, the relative weight of the anchoring constraints on the positions is two orders of magnitude larger than that governing the torsion at nodes.

### 3.5. Analysis

Figures 11 and 12 show the results of the optimization method described in section 3.4 for the three pairs of patterns given on Figure 10 on the two reference surfaces described in section 3.3. Color dots indicate the deviation angle (in degrees) between nodes axes and surface normals, which also corresponds to the kink angle between beams top surfaces and cladding panels. Both denominations will be therefore indifferently used in the following. In both figures, geometrical torsion at node has been limited at 0.5°, an acceptable tolerance for many construction techniques.

For the pair *(a,b),* we observe that for pattern *a*, surface normals naturally give a torsion-free structure (provided that a small tolerance on torsion is allowed). This is due to the alignment of each beam with the principal curvature directions. On the contrary, for pattern *b*, a high deviation of node axes compared to surface normals is necessary to make the structure torsion-free. The average deviation angle is close to 20°, which means that beams top surfaces have an average kink angle of 20° with the surface.

In the pair *(c,d)*, pattern *d*, which is just rotated compared to pattern *b*, has an average kink angle of 12.8 and 15.4° for the two surfaces. However, pattern *c* has a much lower average kink, of 5.4° and 5.1°. The difference is even higher between patterns *e* and *f*. The average kink is nearly 8 times lower on the first reference surface for pattern *e* than for pattern *f,* and more than 9 times lower on the cylinder. We observe that the ratio of average angle between patterns fulfilling and not fulfilling the rules is roughly the same for the two reference surfaces.

Considering then the maximum angle deviation between node normals and surface normals, there is a notable difference in the ratios between the two surfaces. This maximum deviation is due to only a few nodes at the boundaries and would require a specific treatment on a real project.

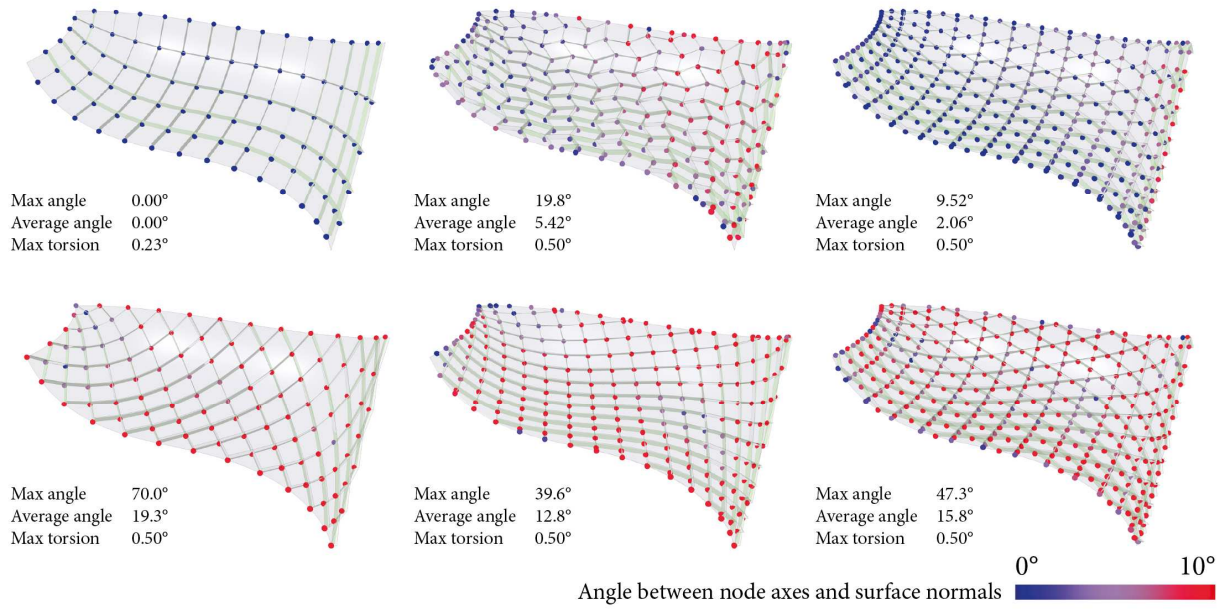


Figure 11. Deviation of the node axes from the surface normals for the six patterns on the first reference surface

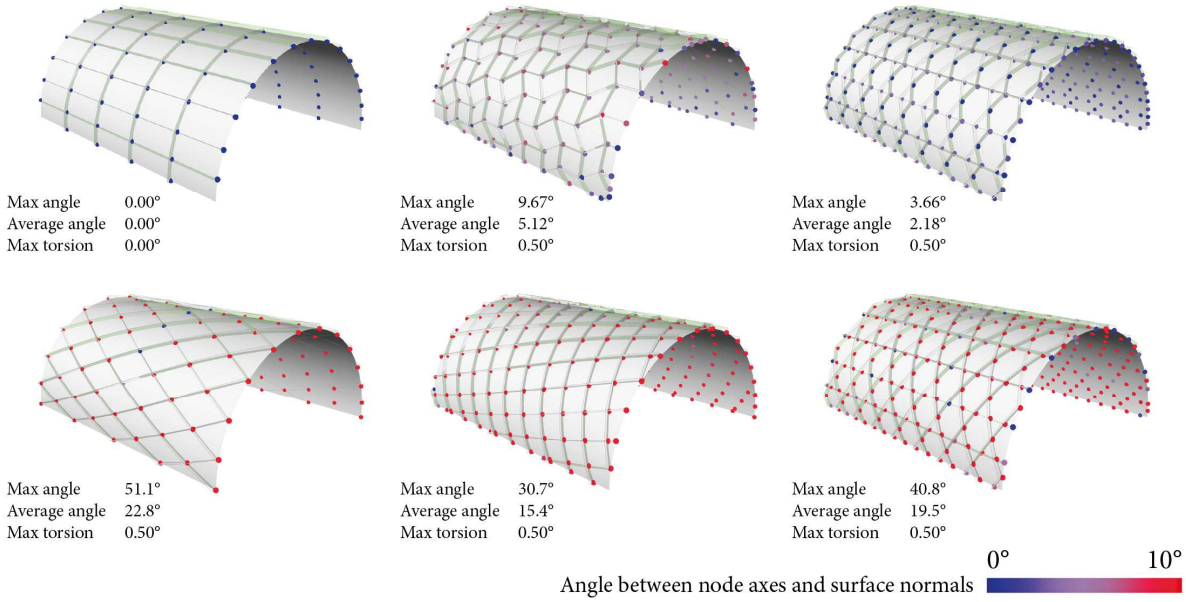


Figure 12. Deviation of the node axes from the surface normals for the six patterns on the second reference surface

### 3.6. Conclusion

With a same tolerance on torsion of 0.5° and the same reference patterns, patterns that fulfills the rules have normals that deviate significantly less (3 to 8 times less) from the surface normals for the three pairs of patterns that we considered. We remark that patterns fulfilling the rules cannot be at the same time torsion-free and have a perfect alignment of node axes with surface normals: there is still a small kink. However, this kink is much more manageable with fabrication tolerances than with patterns not fulfilling it.

## 4.Design examples and discussion

### 4.1. Versatility of the method: shape and pattern

In this section, we show the vast design possibilities offered by patterns fulfilling the rules. Figure 13 shows a surface with planar curvature lines, generated from [16]. The generation steps described in section 3.4 are performed to cover it by an octo-quad pattern. The average deviation of the beams from the surface normals is 1.8°. Figure 14 shows a constant mean curvature surface covered by an Archimedean tri-quad pattern. Because the curvature lines have a singularity at the apex, the pattern also has a singularity at that point: three quadrangles meet at the same point, contrary to the other vertices. The average deviation of node axes is 5.8°. Finally, Figure 15 shows the geometry of a stadium like shape based on a Monge surface, covered by a hex-quad pattern. The average deviation of beams from surface normals is 1.9°.

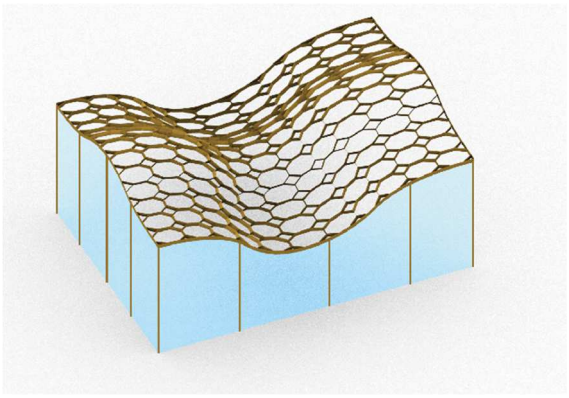

Figure 13. A torsion-free octo-quad pattern

Figure 14. A constant mean curvature surface with a singularity

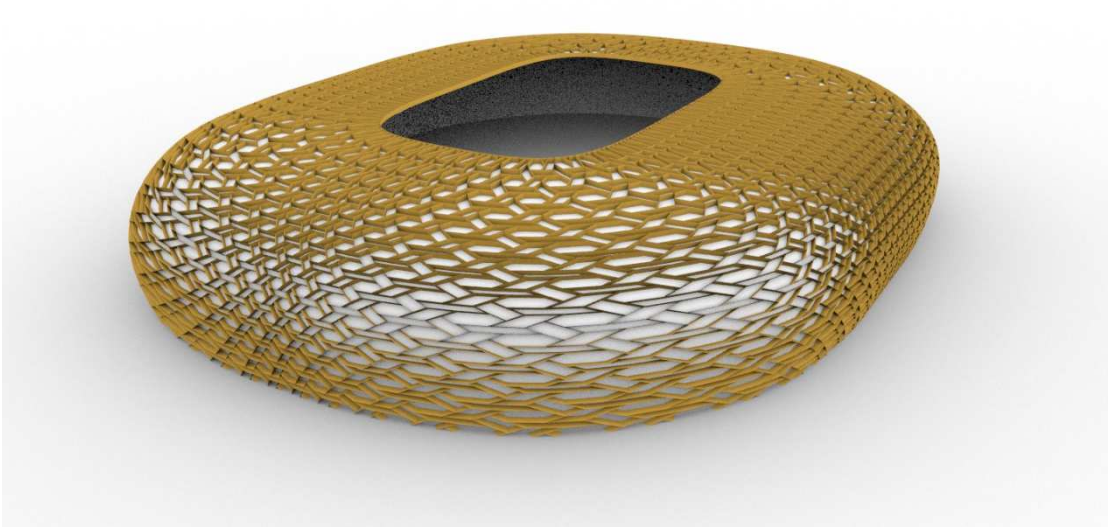

Figure 15. The geometry of a stadium covered by a hex-quad pattern (4th pattern on Figure 8)

### 4.2. Discussion

**Variation of deviation for patterns fulfilling the rules**

On Figures 11 and 12, we observe a significant variation of the deviation of node axes from surface normals for patterns a, c and e, whereas they each fulfill the rules. This variation can be understood qualitatively looking at Figure 16. These two patterns both fulfill the rules. The parallel transformation which results from an elongation of the primitive cell is shown in red at the bottom. As discussed in section 2.1, the surface normals vary linearly at the first order, they are shown in blue. For the left pattern (hexagonal), the distance between nodes axes $N$ and surface normals $n$ is low. However, for the right one, the parallel deformation required to elongate the primitive cell results in a high deformation of the pattern. Consequently, the right tri-quad pattern results in a higher deviation of the nodes axes than the hexagonal one. This explains why a relatively high deviation (5.8°) is observed on the trinoïd of Figure 14 compared to the structures of Figures 13 and 15 (below 2°).

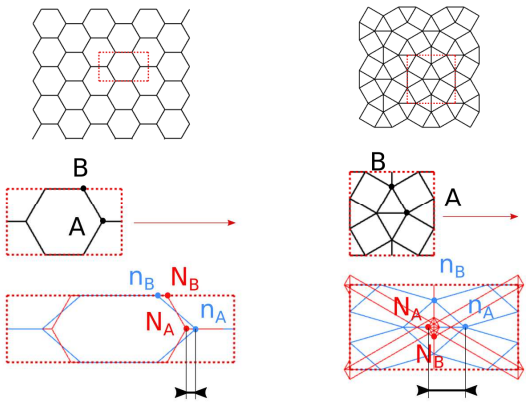


Figure 16. Distance between node axis and surface normal for two patterns

**Importance of edge length and torsion tolerance**

One important geometrical aspect in the deviation of normals is the ratio of edge length over the curvature radius of the surface. Since there is a constant tolerance on torsion, a mesh with infinitely small edges can always be made torsion free, whatever its orientation on a surface and even if it does not fulfill the rules. Figure 17 shows how the average edge

length and the tolerance on torsion both affect the average deviation of node axes compared to surface normals for the zig-zag quad pattern of section 3.3. We observe that smaller edges result in less deviation, and that a lower tolerance on torsion may increase significantly the average deviation. Hence, the relevance of the proposed rules for selecting a pattern is higher for a coarsely discretized surface, with a high ratio of edge length to curvature radius.

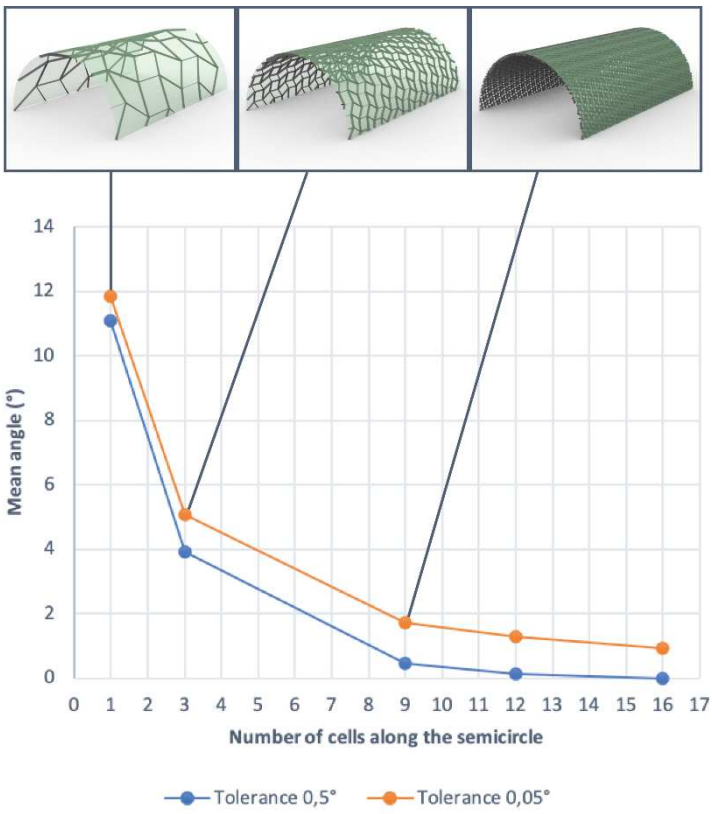


Figure 17. Effect of edge length and torsion convergence criterion on the mean deviation angle between node axes and surface normals for a skew quad pattern on a cylinder.

## 5. Conclusion

We proposed a simple geometrical set of rules to select and orient patterns on a curved surface so that geometries of gridshells without geometrical torsion can be obtained, in which beams are near perpendicular to the envelope surface. The rules pertain to the geometry of the pattern and to its orientation with respect to the principal curvature directions of the surface. They are derived from differential geometry in a linearized asymptotic case, and validated numerically on building-size meshes. It turns out that a great variety of patterns is possible with these properties, thus offering rich design possibilities. Surprisingly, a minor modification of the geometry of a pattern can result in drastic reduction of issues related to nodal torsion.

## Acknowledgements

We warmly thank Thomas Leprisé for his contributions in this work during the class project *Advanced design of structures* at Ecole des Ponts. This work was partially supported by Labex MMCD.

## References

[1] X. Tellier, O. Baverel, C. Douthe, and L. Hauswirth, “Gridshells without kink angle between beams and cladding

panels," *Proc. IASS Symp. 2018 Creat. Struct. Des. Boston, USA*, 2018.

[2] S. Stephan, K. Knebel, and J. Sanchez-Alvarez, "Reticulated Structures On Free-Form Surfaces," *Stahlbau*, vol. 73, no. April, pp. 562–572, 2004, doi: 10.1016/S0924-0136(97)00340-3.

[3] H. Pottmann and J. Wallner, "The focal geometry of circular and conical meshes," *Adv. Comput. Math.*, vol. 29, no. 3, pp. 249–268, 2007, doi: 10.1007/s10444-007-9045-4.

[4] Y. Liu, H. Pottmann, J. Wallner, Y.-L. Yang, and W. Wang, "Geometric modeling with conical meshes and developable surfaces," *ACM Trans. Graph.*, vol. 25, no. 3, p. 681, 2006, doi: 10.1145/1141911.1141941.

[5] X. Tellier *et al.*, "The Caravel heX-Mesh pavilion , illustration of a new strategy for gridshell rationalization," *SN Appl. Sci.*, vol. 2, no. 781, 2020, doi: 10.1007/s42452-020-2561-2.

[6] C. Jiang, J. Wang, J. Wallner, and H. Pottmann, "Freeform honeycomb structures," in *Computer Graphics Forum*, 2014, vol. 33, no. 5, pp. 185–194, doi: 10.1111/cgf.12444.

[7] R. Richter and M. Alexa, "Beam meshes," *Comput. Graph.*, vol. 53, pp. 28–36, 2015, doi: 10.1016/j.cag.2015.08.007.

[8] X. Tellier, "Morphogenesis of curved structural envelopes under fabrication constraints," PhD Thesis, Université Paris-Est, 2020.

[9] C. Jiang, C. Tang, A. Vaxman, P. Wonka, and H. Pottmann, "Polyhedral Patterns," *ACM Trans. Graph.*, vol. 34, no. 6, 2015, doi: 10.1145/2816795.2818077.

[10] A. Vaxman, C. Müller, and O. Weber, "Regular meshes from polygonal paterns," *ACM Trans. Graph.*, vol. 36, no. 4, 2017, doi: 10.1145/3072959.3073593.

[11] A. Schiftner, M. Höbinger, J. Wallner, and H. Pottmann, "Packing circles and spheres on surfaces," *ACM Trans. Graph.*, vol. 28, no. 5, p. 1, 2009, doi: 10.1145/1618452.1618485.

[12] R. Mesnil, C. Douthe, and O. Baverel, "Non-standard patterns for gridshells : fabrication and structural optimization," *J. Int. Assoc. Shell Spat. Struct.*, vol. 58, no. 4, pp. 277–286, 2017.

[13] S. Malek and C. Williams, "Structural Implications of using Cairo Tiling and Hexagons in Gridshells," *Proc. Int. Assoc. Shell Spat. Struct. Symp.*, no. September 2013, pp. 3–6, 2013.

[14] M. P. do Carmo, *Differential geometry of curves and surfaces*. Prentice-Hall, Inc., 1976.

[15] S. Bouaziz, M. Deuss, Y. Schwartzburg, T. Weise, and M. Pauly, "Shape-Up : Shaping Discrete Geometry with Projections," *Eurographics Symp. Geom. Process.*, vol. 31, 2012, doi: 10.1111/j.1467-8659.2012.03171.x.

[16] X. Tellier, C. Douthe, L. Hauswirth, and O. Baverel, "Surfaces with planar curvature lines: Discretization, generation and application to the rationalization of curved architectural envelopes," *Autom. Constr.*, vol. 106, 2019, doi: 10.1016/j.autcon.2019.102880.